Designing a Ce/In-CHA OXZEO catalyst for high-efficient selective catalytic reduction of nitrogen oxide with methane

Chunlei Zhang [a,b], Guangyan Xu [c,*], Yanshuang Zhang [a,b], Chuang Chang [a,b], Miao Jiang [a,b], Luna Ruan [a,b], Min Xiao [a,b], Zidi Yan [a,b], Yunbo Yu [a,b,c,**], Hong He [a,b,c]

[a] School of Rare Earths, University of Science and Technology of China, Hefei 230026, China
[b] Ganjiang Innovation Academy, Chinese Academy of Sciences, Ganzhou 341000, China
[c] State Key Joint Laboratory of Environment Simulation and Pollution Control, Research Center for Eco-Environmental Sciences, Chinese Academy of Sciences, Beijing 100085, China

ARTICLE INFO

ABSTRACT

Selective catalytic reduction of nitrogen oxides with methane (CH_4-SCR) has emerged as a promising technology for mitigating exhaust emissions from natural gas vehicles, while its insufficient catalytic activity and durability are key barriers to application. In this study, novel Ce/In-CHA OXZEO catalysts were prepared, demonstrating exceptional catalytic performance and stability in the CH_4-SCR reaction. Over these OXZEO catalysts, indium species predominantly existed in the form of InO^+ and In_xO_y within the CHA zeolite framework, while CeO_2 nanoparticles primarily resided as an external layer. During the CH_4-SCR reaction, NO oxidation to form NO_2 and nitrate species was triggered by CeO_2, which further enhanced the activation of CH_4 on InO^+ sites, thus boosting the low-temperature CH_4-SCR process by facilitating the formation of the key intermediate CH_3NO_2. The synergy between InO^+ and CeO_2 underscores the exceptional performance and stability of the Ce/In-CHA with a low SiO_2/Al_2O_3 ratio in reducing NOx and CH_4 emissions.

1. Introduction

Nitrogen oxides (NOx) and methane (CH_4) emissions from natural gas-fueled engines are significant environmental concerns. NOx contributes to atmospheric pollution, while CH_4 is a potent greenhouse gas [1]. The co-presence of NOx and VOCs will cause several air pollutants, including ozone (O_3), fine inhalable particles ($PM_{2.5}$), and other secondary pollutants [2]. Selective catalytic reduction of NOx with hydrocarbon (HC-SCR) is a desirable technology to synergistic control of NOx and hydrocarbon, and thus has attracted extensive research interest [3–5]. In particular, selective catalytic reduction of NOx with methane (CH_4-SCR) has garnered considerable attention as a technology to simultaneously control NOx and CH_4 emissions in natural gas vehicle exhaust [6–8]. This approach holds great promise for addressing these environmental challenges.

Generally, HC-SCR reaction involves the activation of hydrocarbons to form reactive oxygenated hydrocarbons, which further reacts with NOx and/or nitrate to yield organo−NOx compounds, and subsequently

reduces to generate N_2, CO_2, and H_2O [9–11]. The activation of CH_4 is also the initial step of CH_4-SCR reaction, the occurrence of which is hindered by highly stable C-H bonds and nonpolar tetrahedral geometry [12]. As a result, highly active CH_4-SCR catalysts are required to contain the active sites for the activation of CH_4 at low temperature. To this aim, previous studies revealed that In-containing zeolites were active for CH_4-SCR [13–19]. Grünert et al. investigated the relationship between the structure of indium sites and their catalytic properties and found that indium-oxo species within the ZSM-5 zeolite are active sites, but the In-Silicate catalysts activated only methane and did not reduce NO, suggesting that their catalytic properties also depend on the content of Brønsted acid in the zeolite [19]. To enhance strong Brønsted acid, In/H-Beta with proline was synthesized, the presence of which promoted the indium-skeleton interaction, and improved the water and sulfur resistance for the CH_4-SCR reaction [18]. Nevertheless, the low activity of single-component catalysts precludes their application.

To increase the CH_4-SCR performance of the catalysts, previous studies found that NO_2 was beneficial for CH_4 activation to generate

---

organic nitrogen compounds, the latter of which is key intermediate of NOx reduction by methane. To realize such NO$_2$ assisted CH$_4$ activation process, modifications by a second transition metal, e.g., Pd [20], Ce [17,21], Co [22–24], and Ru [25], were also known as a feasible strategy. For instance, the addition of Co into In-containing H-ZSM-5 had been found to increase the rate of NO$_2$ production, thereby enhancing the formation of InNO$_3$/NO$^+$ species, ultimately improving the performance for CH$_4$-SCR [23]. Similar synergy between Ru and In had been observed on H-CHA, and the addition of Ru species promoted the oxidation of NO to form NO$_2$, thus enhancing the CH$_4$-SCR reaction [25]. Additionally, the strategy of nanoscale-separated active sites allowed for tandem reactions by adjusting the match and intimacy between active sites [26–28]. In this nanoscale-separated system developed for CH$_4$-SCR, NO activation and C-N coupling occurred at two different active sites, thus benefiting NOx reduction. Maunula et al. investigated a novel multifunctional catalyst combination of In/ZSM-5 and Pt/Al$_2$O$_3$, in which the presence of Pt/Al$_2$O$_3$ enhanced the formation of NO$_2$, thus promoting the formation of partially oxidized, nitrogen-free and nitrogen-containing methane derivatives [29]. Similarly, the catalytic system consisting of Ce/HZSM-5 and CoOx exhibited a significant improvement in the CH$_4$-SCR reaction by facilitating the oxidation of NO to NOx [30]. Zhu et al. demonstrated that the addition of Ga$_2$O$_3$ can improve the dispersion of Co$_3$O$_4$, leading to increased exposure of InO$^+$ sites, which, in turn, improved the oxidation of NO [31].

Ceria has been widely used as an active component in the NOx storage and reduction process due to its remarkable redox property and oxygen storage capacity [32]. When combined with In-containing zeolite, ceria can serve as NO oxidation active sites in CH$_4$-SCR and help store nitrate species. In addition, CHA zeolite as a carrier, which had been commercially used in NH$_3$-SCR [25,33,34], could effectively inhibit the adverse effects of water vapor in the exhaust of natural gas vehicles [35] and ultimately enhance the overall catalyst performance.

Inspired by these speculations as mentioned above, in this study, a series of oxide-zeolite (abbreviated as OXZEO thereafter) catalysts were synthesized through a self-assembly method using CHA zeolites as the core support for indium species, with an external layer of CeO$_2$. As expected, these catalysts exhibited remarkable performance in the CH$_4$-SCR reaction under both the presence and absence of water. CeO$_2$ played a crucial role in enhancing the oxidation of NO, whereas InO$^+$ species were actively involved in the activation of CH$_4$. This work shed new light on the design of CH$_4$-SCR catalysts and the simultaneously control NOx and CH$_4$ emissions.

2. Experimental section

2.1. Catalyst preparation

All reagents were analytical grade and used without further purification. Indium nitrate hydrate (In(NO$_3$)$_3$·xH$_2$O, 99.99% metals basis), ammonium chloride (NH$_4$Cl, 99.5%) and cerium nitrate hydrate (Ce(NO$_3$)$_3$·6H$_2$O, 99.5% metals basis) were purchased from Aladdin Reagent Co Ltd. Hexamethylenetetramine (HMT) was obtained from Xilong Scientific Co., Ltd. The CHA zeolites (Na-SSZ-13, SiO$_2$/Al$_2$O$_3$ = 12/20/50, nanoscale) was purchased from the Raodong (Liaoning) New Material Co., Ltd.

2.1.1. Synthesis of In-CHA

The synthesis of In-CHA-x (SiO$_2$/Al$_2$O$_3$ =12, 20, 50) involved a liquid ion exchange process conducted as follows. Initially, the CHA zeolites were mixed with a NH$_4$Cl aqueous solution (100 mL, 1.0 M) under vigorous stirring for 4 h at 80 °C. Subsequently, the resulting material was vacuum-filtered, washed with deionized water, and dried overnight at 100 °C. This ammonium exchange procedure was repeated three times for thoroughness. H-CHA was obtained by calcining NH$_4$-CHA at 500 °C for 2 h. After ammonium exchange, the obtained NH$_4$-CHA sample was combined with a solution containing 0.21 g of In(NO$_3$)·

xH$_2$O precursors and 100 mL of deionized water. After stirring at 80 °C for 8 h, slurry was obtained, and the water was removed in a rotary evaporator at 80 °C at reduced pressure. The sample was subsequently dried and calcined at 500 °C in air for 1 h. Following this, it was subjected to reduction in a 5% H$_2$/N$_2$ atmosphere at 500 °C for 1 h, followed by re-oxidation in air at 500 °C for 2 h. These obtained In-exchanged zeolites denoted as In-CHA-12, In-CHA-20, and In-CHA-50.

2.1.2. Synthesis of Ce/CHA

The Ce/CHA-12 was prepared by a self-assembly method using the functional groups of hexamethylenetetramine (HMT) to create a core-shell structure. 1 g of CHA-12 was dispersed in an 80 mL mixed solution of water and ethanol (v/v = 1), and then ultrasound for 30 min. Afterward, 0.62 g of Ce(NO$_3$)$_3$·6H$_2$O and 0.85 g of HMT were added sequentially, followed by continuous stirring and reflux for 2 h at 80 °C. The product was obtained through centrifugation, washing, drying, and calcining in an airy environment at 500 °C for 2 h. The final product was donated as Ce/CHA-12.

2.1.3. Synthesis of Ce/In-CHA

The Ce/In-CHA OXZEO catalysts were prepared by the same procedures as in the synthesis of Ce/CHA-x, except for substituting CHA with In-CHA. The final product was named as Ce/In-CHA-x, where x presents the SiO$_2$/Al$_2$O$_3$ ratio, that is, 12, 20 and 50 in this work.

2.2. Catalyst characterization

X-ray diffraction (XRD) patterns were acquired using a Bruker D8 Advance diffractometer with Cu Kα radiation (λ = 1.5418 Å, 40 kV, 40 mA) with a step size of 0.02 °. Nitrogen sorption isotherms were measured at − 196 °C using a Micromeritics ASAP 2460 system. The samples were degassed for 8 h at 300 °C before performing the measurements. The Brunauer-Emmett-Teller (BET) surface areas were calculated from the adsorption data. High resolution-transmission electron microscopy (HR-TEM) characterization were performed on a JEOL JEM-F200 with an acceleration voltage of 200 kV. Energy dispersive spectroscopy (EDS) elemental maps was obtained on a JED-2300T. The light absorption spectra were recorded by using UV–vis diffuse reflectance spectra (UV-3600i Plus). The content of In and Ce was measured using inductively coupled plasma optical emission spectroscopy (ICP-OES) on an Agilent ICPOES730 instrument. X-ray photoelectron spectra (XPS) were obtained with a Thermo Fisher Scientific ESCALAB 250Xi photoelectron spectroscopy system, using a monochromatic Al Kα (1486.6 eV) X-ray source. The binding energy values were calibrated using the C1s peak at 284.8 eV.

NH$_3$ temperature programmed desorption (NH$_3$-TPD) analysis was performed on a Micromeritics AutoChem II 2920 apparatus equipped with a thermal conductivity detector (TCD). A 50 mg sample was pretreated in a 2% O$_2$/N$_2$ flow (30 mL/min) at 500 °C for 1 h. After cooling to 50 °C, the sample was saturated with NH$_3$, and then Ar flow was introduced as the sweep gas. Finally, NH$_3$-TPD profile was then recorded across the temperature range of 50 to 600 °C at a rate of 10 °C/min. For the H$_2$ temperature programmed reduction (H$_2$-TPR) test, the samples were pretreated in a 2% O$_2$/N$_2$ flow (30 mL/min) at 500 °C for 1 h. After cooling to 50 °C, the gas composition was switch to a 5% H$_2$/Ar gas mixture (30 mL/min), and the experiment was performed from 50 to 900 °C at a rate of 10 °C/min.

2.3. Catalytic study

The CH$_4$-SCR reactions were performed using packed catalysts (0.28 mL, 40–60 mesh) in a fixed-bed quartz reactor at atmospheric pressure. These experiments utilized a reactant gas mixture composed of 2000 ppm CH$_4$, 1200 ppm NO, 4% O$_2$, and 10% H$_2$O (when added) in N$_2$ balance. The gas hourly space velocity (GHSV) was controlled in the range of 18,000 h^{-1} to 130,000 h^{-1} (85 mL/min) by changing the catalyst

volume. The concentrations of NO, NO_2, CH_4, N_2O, and CO were analyzed by an FTIR spectrometer (Nicolet Nexus iS50) equipped with a 2.4 m PIKE gas cell. The NOx and CH_4 conversions were calculated using the following equations.

$$NO_x\ Conversion(\%) = \frac{[NO_x]_{in} - [NO_x]_{out}}{[NO_x]_{in}} \times 100\%$$

(NOx represents NO and NO_2)

$$CH_4\ Conversion(\%) = \frac{[CH_4]_{in} - [CH_4]_{out}}{[CH_4]_{in}} \times 100\%$$

$$N_2\ selectivity = (1 - \frac{2 \times [N_2O]_{out}}{[NO_x]_{in} - [NO_x]_{out}}) \times 100\%$$

where the subscripts "in" and "out" represented the gas concentration at the inlet and outlet under steady state, respectively.

The reaction kinetics of CH_4-SCR were also measured in the above fixed-bed reactor. Both internal diffusion and external mass transfer resistances in the reaction were carefully eliminated, and the detailed process could be found in Fig. S18. The NOx conversion was kept at < 20% by adjusting the volumetric space velocity of 100,000 h^{-1}, allowing for the calculation of the apparent activation energy (Ea) and the reaction rate (r) from the NO/CH_4 conversion, as follows:

$$\gamma = \frac{F_{NO_x} \times X_{NO_x}}{W_{cat}}$$

$$k = Ae^{-\frac{Ea}{RT}}$$

where F_{NO_x} represents the NOx flow rate (mol/s), X_{NO_x} represents the NOx conversion, W_{cat} (g) is the mass of the catalyst, NOx represents NO and NO_2. The equation for the reaction rate for NO was calculated as follows:

$$\gamma_{NO} = k[NO]^{\alpha}[CH_4]^{\beta}$$

where γ_{NO} is the conversion rate of NO; k is the reaction rate constant; α and β are the reaction orders of NO and CH_4, respectively; [NO] and [CH_4] are the concentrations of NO and CH_4, respectively.

2.4. In-situ DRIFTS spectra

In-situ DRIFTS experiment was carried out on an FTIR spectrometer (Thermo Nicolet iS50) equipped with a Harrick cell and a high-sensitivity MCT detector. Each spectrum was obtained by accumulating 32 scans with a resolution of 8 cm^{-1}. Before each test, the sample was pretreated at 500 °C in 20% O_2 + Ar for 1 h, followed by a cooling process to 400 °C. The background spectrum at the desired temperature
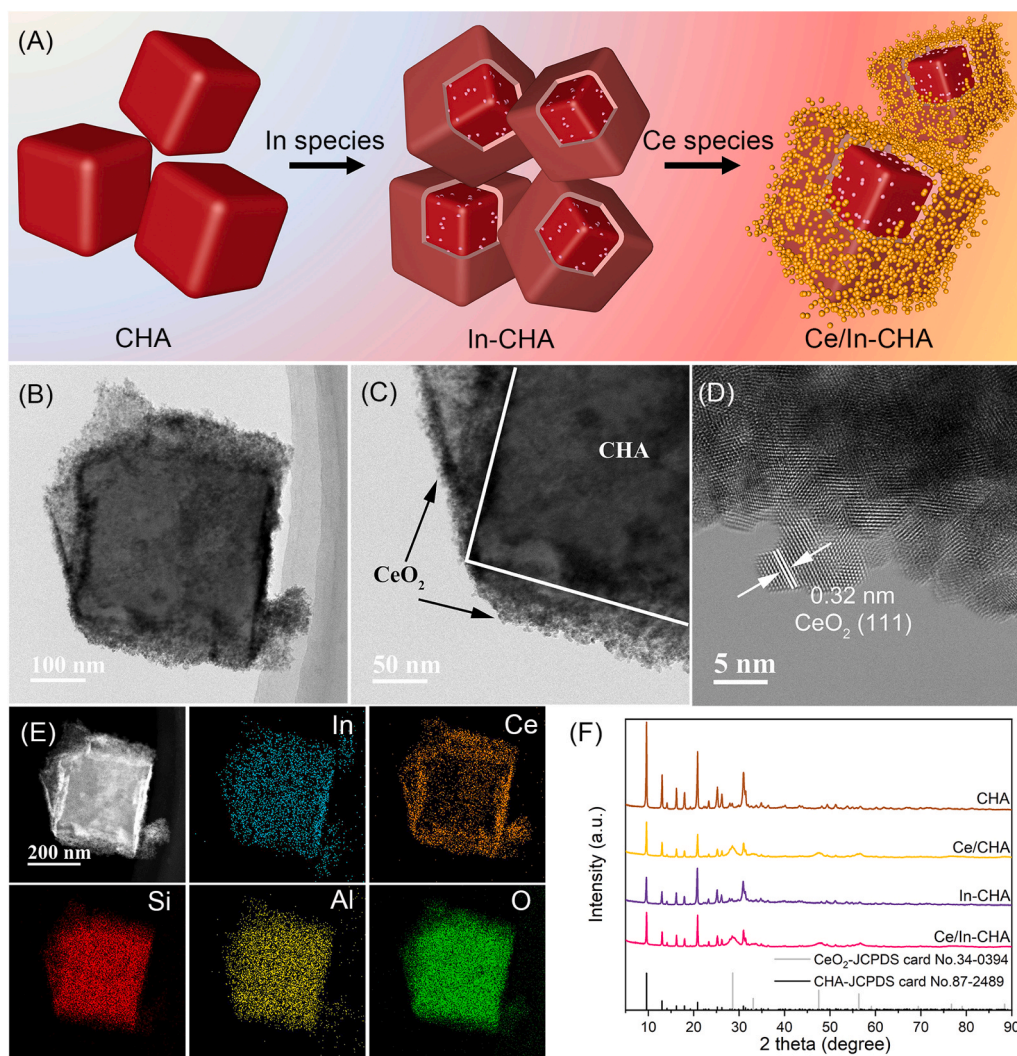

Fig. 1. Schematic illustration of the preparation of Ce/In-CHA OXZEO catalysts (A); HR-TEM images of Ce/In-CHA-12 (B, C, D); HAADF-STEM image and element mappings of Ce/In-CHA-12 (E); XRD patterns of zeolite catalysts (F).

was collected after the pretreatment under a Ar atmosphere. The co-adsorption of NO + CH$_4$ + O$_2$ was carried out by adsorbing a mixture of 2000 ppm CH$_4$, 1200 ppm NO, and 4% O$_2$ at 400 °C for 1 h. For the transient reactions, the catalysts were exposed to a mixture of 2000 ppm CH$_4$ + 4% O$_2$ (or 1200 ppm NO + 4% O$_2$) at 400 °C for 30 min, followed by purging in Ar until the signal was constant. Subsequently, the flow of 1200 ppm NO + 4% O$_2$ (or 2000 ppm CH$_4$ + 4% O$_2$) was introduced, and the resulting spectra were recorded.

3. Results and discussion

3.1. Catalyst characterization

Fig. 1A illustrates the preparation procedure of Ce/In-CHA OXZEO catalysts. As shown in Fig. S1, the CHA zeolite exhibited typical cubic crystals with diameter of hundreds nanometer. On the In-CHA, indium species was highly dispersed inside the CHA zeolite without any lattice fringing detected. In contrast, CeO$_2$ grows on the surface of zeolite over Ce/CHA, with numerous small nanoparticles observed, forming a core-shell structure. Similarly, on the Ce/In-CHA (Fig. 1D), lattice spacing (0.32 nm) assigned to CeO$_2$ (111) was also observed on the zeolite surface [36]. EDS elemental mapping images (Fig. 1E) revealed that indium species mainly distributed inside the CHA zeolite, while Ce were primarily distributed around the zeolite. Line scanning analysis (Fig. S2) further confirmed the reverse dispersion of indium species and cerium species, demonstrating the core-shell structure of OXZEO catalysts. Besides, the Ce/In-CHA samples with higher SiO$_2$/Al$_2$O$_3$ ratio showed similar structure with the Ce/In-CHA-12 (Fig. S3).

The XRD patterns (Fig. 1F and S4) showed that the characteristic diffraction peaks of CHA structure were present on these zeolite catalysts (JCPDS card No. 87–2489) [37,38]. However, the migration of indium species has had an impact on the CHA channel structure, resulting in reduced diffraction peak intensity for In-CHA-12 (Fig. 1F). Unfortunately, the state of the indium species could not be discerned via XRD due to their small particle size or highly dispersed distribution. Furthermore, the XRD analysis revealed the presence of diffraction peaks corresponding to CeO$_2$ (JCPDS card no. 34–0394) in the Ce/CHA-12 catalyst, with an overall reduction in diffraction peak intensity. This reduction is attributed to the distribution of CeO$_2$ particles covering the crystal structure of CHA-12. Similarly, only diffraction peaks of both CHA and CeO$_2$ were observed on the Ce/In-CHA-12 [39]. Notably, as the SiO$_2$/Al$_2$O$_3$ ratio increased, the XRD results resemble those observed for Ce/In-CHA-12.

The nitrogen adsorption-desorption isotherms exhibited a characteristic adsorption curve of type I plus IV on the above catalysts (Fig. S5), signifying the presence of a highly developed micro/mesoporous structure [40,41]. As indicated in Table 1, the CHA-12 zeolite exhibited a specific BET surface area of 568 m^2/g and a pore volume of 0.31 cm^3/g. In contrast, In-CHA-12 (511 m^2/g), Ce/CHA-12 (481 m^2/g), and Ce/In-CHA-12 (494 m^2/g) showed lower specific BET surface areas. Compared to CHA-12 zeolite, the microporous surface area of Ce/In-CHA-12 catalyst was reduced from 555 to 450 m^2/g, possibly due to partial blockage of the micropores within zeolite by deposited indium species and cerium species. Notably, alterations in the SiO$_2$/Al$_2$O$_3$ ratio have minimal impact on the specific surface area of the catalysts. After catalytic test, only slight decreases in the specific surface area and pore volume (less than 10%) were observed on the Ce/In-CHA-12, indicative of its structural stability. Furthermore, XRF and ICP-OES analyzes provided additional confirmation that the structure and composition of the synthesized samples closely matched the theoretical values.

NH$_3$-TPD measurements were conducted to assess the quantity and strength of acid sites in these catalysts. As depicted in Fig. 2A and Fig. S6, all the samples exhibited four distinct NH$_3$ desorption peaks within the temperature range of 50–600 °C. Peak α (105 °C) was associated with surface hydroxyl groups, such as Si-OH and Al-OH [42].

Table 1
Chemical, textural properties of zeolite catalysts.

Sample	S$_{BET}$ (m^2/g)	S$_{micro}$ (m^2/g)	V$_{total}$ (cm^3/g)	V$_{micro}$ (cm^3/g)	SiO$_2$/Al$_2$O$_3$ (mol/mol)[a]	In (wt %)[b]	Ce (wt %)[b]
CHA-12	568	555	0.31	0.27	11.8	-	-
In-CHA-12	511	483	0.29	0.24	12.4	6.1	-
Ce/CHA-12	481	445	0.29	0.22	11.6	-	13.0
Ce/In-CHA-12	494	450	0.31	0.22	11.8	5.7	13.1
Ce/In-CHA-20	455	429	0.26	0.21	19.3	5.7	10.7
Ce/In-CHA-50	467	423	0.28	0.21	44.4	5.4	13.6

[a] Measured by XRF.
[b] Determined by ICP-OES.

Peaks β (145 °C) and θ (230 °C) corresponded to NH$_3$ bonded to weak and strong Lewis acid sites, respectively, while peak γ (400 °C) was attributed to NH$_3$ adsorbed on strong Brønsted acid sites (Si-OH-Al and [InOH]$^{2+}$/[In$_2$(OH)$_4$]$^{2+}$ cation) [43–47]. Upon deconvoluting the NH$_3$-TPD curve, it was determined that the number of acid sites on CHA-12 amounted to 1095 μmol/g. Notably, In-CHA-12 displayed an increased count of acid sites, reaching 1505 μmol/g, particularly the strong Brønsted acid sites, which increased from 221 to 543 μmol/g (Table S1). On the other hand, the introduction of cerium species led to a slight reduction in the number of acid sites on both Ce/CHA-12 (814 μmol/g) and Ce/In-CHA-12 (1320 μmol/g), attributed to the CeO$_2$ coverage on the zeolite surface. Additionally, as the SiO$_2$/Al$_2$O$_3$ ratio increased, the number of acid sites in Ce/In-CHA-20 (1026 μmol/g) and Ce/In-CHA-50 (420 μmol/g) gradually decreased, particularly in the case of Brønsted acids.

The chemical state of the surface components in these catalysts was examined using XPS. As shown in Fig. 2B and Fig. S7A, the binding energies centered at 444.6 and 446.2 eV were attributed to In$_2$O$_3$ species and InO$^+$ species, respectively [18,48,49]. In the In-CHA-12 catalyst, only InO$^+$ species were present, while both In$_2$O$_3$ species and InO$^+$ species were observed on the Ce/In-CHA-12 catalysts (Fig. S7A). The percentage of InO$^+$ species on Ce/In-CHA-12 significantly decreased after the introduction of Ce, possibly due to the interaction between In and Ce species. Considering that XPS is a surface-sensitive technique with a nominal sampling depth of ≤ 10 nm, the appearance of In$_x$O$_y$ species was possibly due to the slightly affected by CeO$_2$ on the external layer of CHA zeolite. The percentage of InO$^+$ species in the Ce/In-CHA-12 catalyst was 10.5% (Fig. S7A), while it gradually decreased to 8.3% in Ce/In-CHA-20 and 5.9% in Ce/In-CHA-50, respectively. This reduction was primarily associated with the decreased content of Brønsted acid sites within the zeolite.

Fig. 2C and Fig. S7B showed Ce 3d XPS spectrum of all catalysts, which was deconvoluted into ten peaks arising from Ce^{4+} (μ''', μ'', μ, υ''', υ', and υ) and Ce^{3+} (μ', μ^0, υ', and υ^0) [36,50]. Based on the fitting results, the percentage of Ce^{3+} on Ce/CHA-12 and Ce/In-CHA-12 catalysts were 41.7% and 44.0%, respectively. With the increased ratio of SiO$_2$/Al$_2$O$_3$ on Ce/In-CHA-x catalysts, the surface Ce^{3+} percentage decreased from 44.0% to 38.6% (Fig. S7B). It is known that the presence of Ce^{3+} species can result in the formation of oxygen vacancies over Ce/In-CHA-x catalysts. The more is Ce^{3+}, the easier to form oxygen vacancies, and the more advantageous is the adsorption of oxygen on the catalyst surface to form chemisorbed oxygen species.

H$_2$-TPR analysis was employed to investigate the redox properties of these catalysts, and the corresponding results were depicted in Fig. 2D
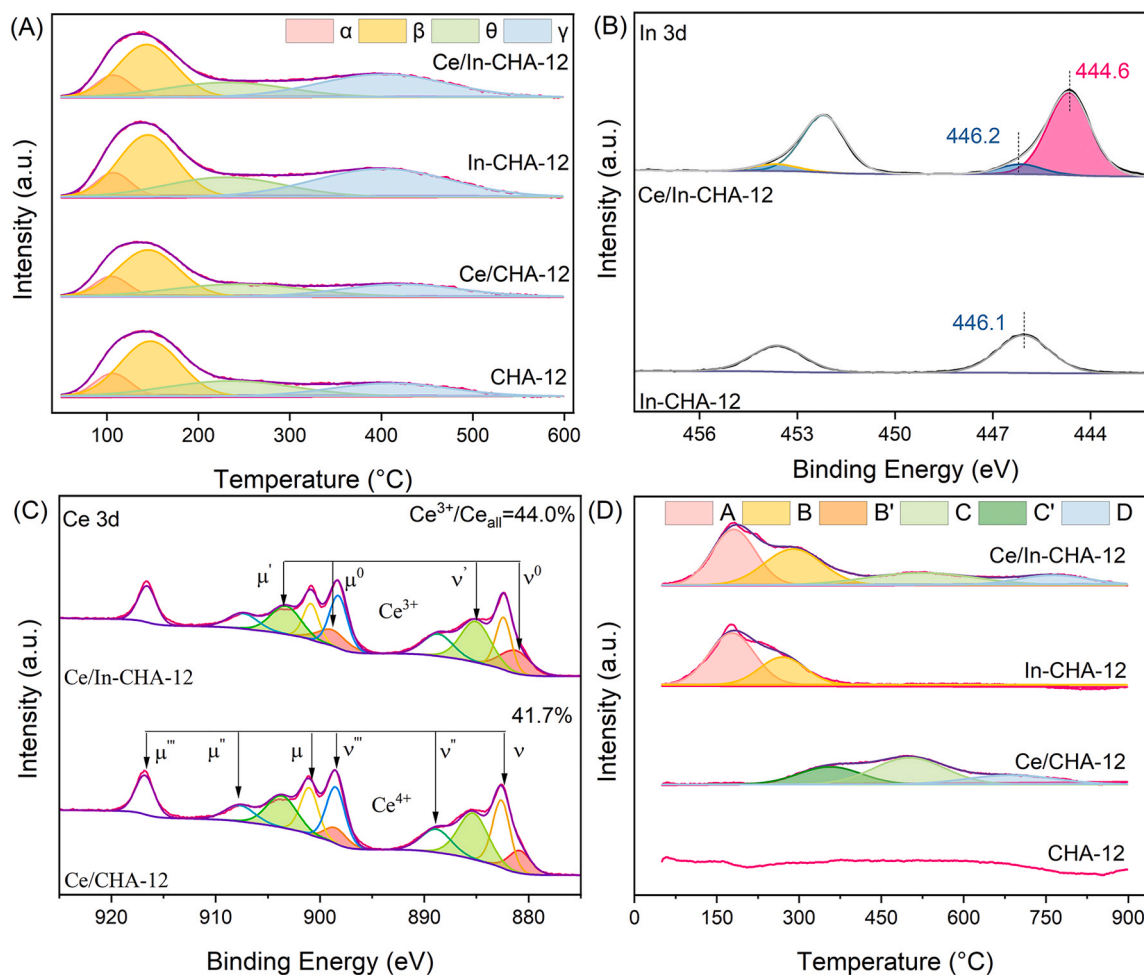
Fig. 2. NH_3-TPD profiles (A), XPS spectra In 3d (B) and Ce 3d (C), and H_2-TPR profiles (D) of zeolites catalysts.

and **S8** and Table S2. The CHA-12 did not exhibit any distinct reduction peak (Fig. 2**D**), while reduction peak A ($< 200\,°C$) and peak B (200–$300\,°C$) attributed to InO^+ and In_xO_y species, respectively, could be observed on the In-CHA-12 sample [14,17,23]. On the other hand, Ce/CHA-12 displayed reduction peaks corresponding to interactions between CeO_2 with the zeolite (peak C', $356\,°C$), surface-trapped oxygen ($Ce^{4+} \rightarrow Ce^{3+}$) (peak C, 500–$600\,°C$), and bulk lattice oxygen (peak D, 600–$800\,°C$) [51,52]. In addition to the aforementioned peaks, the Ce/In-CHA OXZEO catalysts revealed reduction peaks for In_2O_3 nanoparticles (peak B', 350–$500\,°C$) and bulk In_2O_3 (peak E, $> 800\,°C$).

Indium species were distinguished into InO^+, In_xO_y clusters, and In_2O_3 nanoparticles in H_2-TPR, with the H_2 consumption for each species calculated and detailed in Table S2. For the In-CHA-12 catalyst, the H_2 consumption of InO^+ species and In_xO_y species was 466 μmol/g and 249 μmol/g, respectively, with no other species consuming hydrogen. This suggested that indium species primarily existed in a highly dispersed form and as clusters in In-CHA-12. The H_2 consumption of InO^+ for the Ce/In-CHA-12 catalyst (458 μmol/g) matched that of In-CHA-12. However, as the SiO_2/Al_2O_3 ratio increased to 20 and 50, the H_2 consumption of the InO^+ species decreased to 335 and 212 μmol/g, respectively, with the simultaneous appearance of reduction peaks for In_2O_3 nanoparticles and bulk In_2O_3. Furthermore, the hydrogen consumption attributed to the surface-trapped oxygen from CeO_2 in Ce/In-CHA-x catalysts significantly decreased from 247 μmol/g (Ce/In-CHA-12) to 162 μmol/g (Ce/In-CHA-20) and 164 μmol/g (Ce/In-CHA-50). This reduction indicates a decrease in the percentage of Ce^{3+}, consistent with the results of Ce 3d XPS.

To examine the state of indium and cerium species on these zeolite

catalysts, UV–vis analysis was conducted (Fig. S9). Both In-CHA-12 and Ce/CHA-12 samples exhibited a similar absorption edge at around ~300 nm, with a substantial overlap in their absorption spectra. As a result, the absorption characteristics of Ce/In-CHA-12 showed very little difference from those of Ce/CHA-12. Notably, a noticeable redshift of the absorption band edge was observed in Ce/In-CHA-12, Ce/In-CHA-20, and Ce/In-CHA-50. This shift suggested that the In_2O_3 on the support increased in size as the SiO_2/Al_2O_3 ratio was increased [47].

3.2. Catalytic activity

Fig. 3 presents the NO*x* conversion and CH_4 conversion over OXZEO catalysts in CH_4-SCR reaction. In Fig. 3**A-B**, the CHA-12 catalyst displayed minimal NO*x* and CH_4 conversion performance, while the introduction of both indium and cerium species led to significant performance enhancements. The In-CHA-12 catalyst achieved NO*x* conversion of less than 80% but could completely remove CH_4 at $500\,°C$. On the other hand, the Ce/CHA-12 catalyst reached no more than 80% conversion for both NO*x* and CH_4 at $600\,°C$, indicating that the CH_4 activation was associated with the indium species. The Ce/In-CHA-12 exhibited the highest NO*x* catalytic activity, achieving 100% conversion in the temperature range of 395–$600\,°C$. Compared with other zeolite catalysts in the literature to date [1,7,18,25,30,31,49,53,54], the Ce/In-CHA-12 demonstrated to be one of the most promising catalysts for CH_4-SCR reaction applications. Simultaneously, CH_4 conversion increased with rising temperature, reaching 100% at $580\,°C$. Importantly, the SiO_2/Al_2O_3 ratio of CHA had a notable influence on the catalytic performance of Ce/In-CHA-x catalysts (Fig. 3**C-D**). The NO*x*
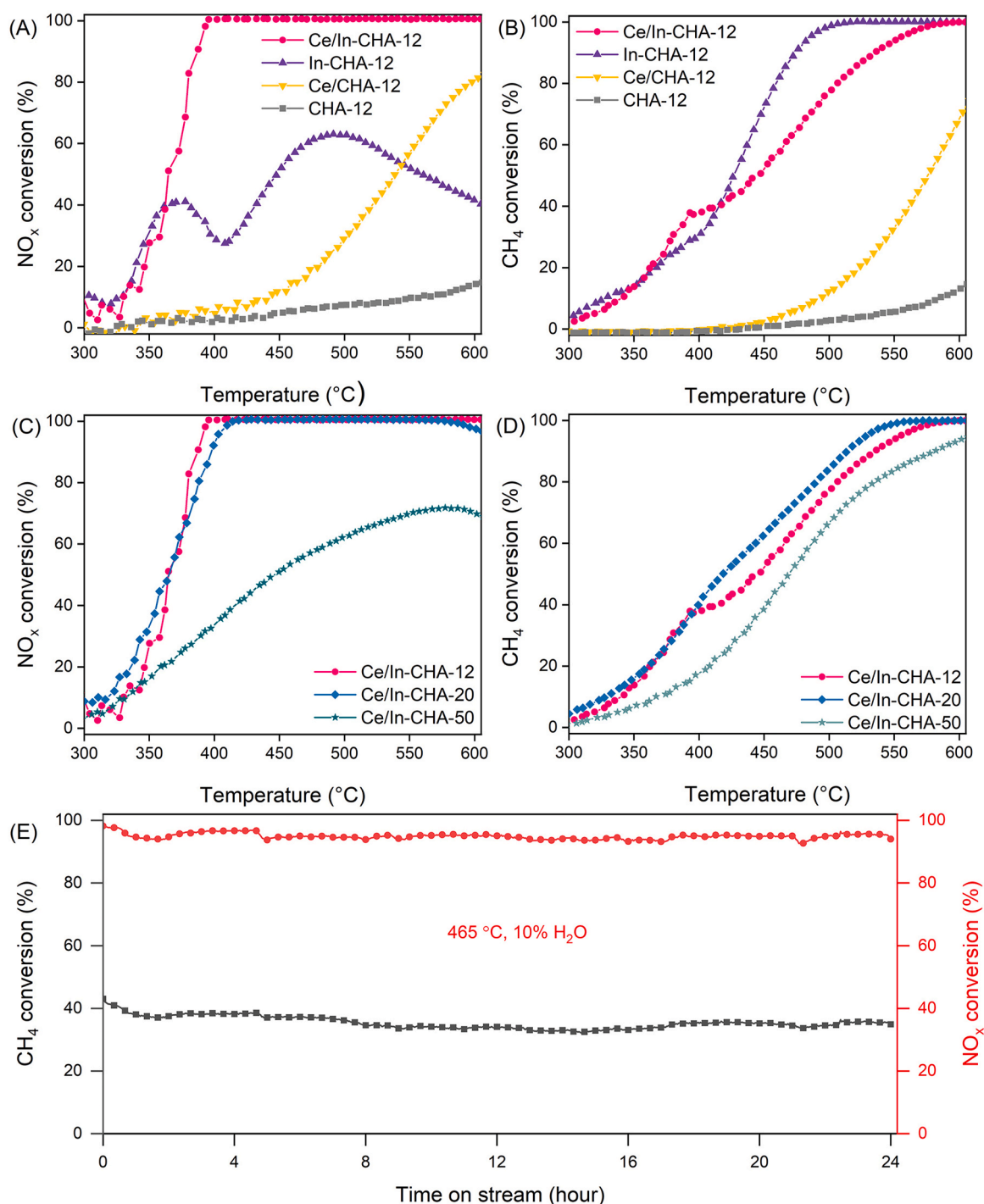
Fig. 3. NOx conversion (A, C) and CH$_4$ conversion (B, D) over different zeolite catalysts in dry CH$_4$-SCR reaction. The stability of Ce/In-CHA-12 in wet CH$_4$-SCR reaction at 465 °C (E). Reaction conditions: 1200 ppm NO, 2000 ppm CH$_4$, 4% O$_2$, and 10% H$_2$O (when added) in N$_2$ balance.

conversion of the Ce/In-CHA-20 catalyst, for example, was slightly lower than that of Ce/In-CHA-12 but still reached 100% at 415 °C. Conversely, Ce/In-CHA-50 achieved no more than 80% NOx conversion and poor CH$_4$ conversion until 600 °C. This was mainly due to the lowest content of acidic sites among the Ce/In-CHA samples with different SiO$_2$/Al$_2$O$_3$ ratios, leading to the formation of In$_x$O$_y$ clusters and bulk In$_2$O$_3$ species (Fig. 2**A and D**). The enrichment of these inactive indium species thereby reduced the ability of Ce/In-CHA-50 for CH$_4$ activation and NOx reduction. During the CH$_4$-SCR reaction, N$_2$ selectivity increased gradually with rising reaction temperature, reaching approximately 100% above 400 °C (Fig. S10). Among these samples,

Ce/In-CHA-12 exhibited the highest N$_2$ selectivity, with the doping of indium species enhancing N$_2$ selectivity.

However, it's noteworthy that the activity of all catalysts experienced a significant decline when the feed contained 10% water vapor (Fig. S11). In the presence of water, the NOx conversion of In-CHA-12 and Ce/CHA-12 catalysts did not surpass 30% within the whole temperature range (Fig. S11A). Nonetheless, In-CHA-12 still achieved 100% CH$_4$ conversion at 570 °C; at this temperature, while Ce/CHA-12 only reached 20% CH$_4$ conversion (Fig. S11B). Under wet CH$_4$-SCR conditions over Ce/In-CHA-12, differently, complete NOx conversion was achieved at the temperatures above 475 °C (Fig. S11A), which was 80 °C

higher than that in the absence of water vapor. Compared with Ce/In-CHA-12, the suppression of water vapor was more pronounced over Ce/In-CHA-20, with 100% NOx conversion achieved at 531 °C (Fig. S11C), which was 116 °C higher than that under dry conditions. Serious suppression due to water vapor was also observed over the Ce/In-CHA-50, exhibiting only 35% NOx conversion and 70% CH$_4$ conversion at the high temperature of 600 °C. These results suggested that water vapor might occupy the active sites of the catalyst, thereby impacting both NOx and CH$_4$ removal performance. Even in the presence of 10% H$_2$O, however, it should be noted that the Ce/In-CHA-12 catalyst maintained considerable catalytic activity at a high GHSV of 130,000 h^{-1} (Fig. S12). During wet CH$_4$-SCR reaction at different temperatures (430 °C and 465 °C), this catalyst also showed excellent stability, without obvious decrease in NOx conversion even after running for 24 h (Fig. 3E and Fig. S13). Such excellent stability of Ce/In-CHA-12 was further confirmed by cycling tests in the presence/absence of water (Fig. S14), during which NOx conversions were only slightly decreased whereas the conversions of CH$_4$ were affected to a certain extent. After pre-sulfurization at 400 °C for 10 h (Fig. S15A), the low temperature activity of Ce/In-CHA-12 for NOx conversion slightly affected, with the T$_{50}$ slightly shifting towards a high temperature of 9 °C (from 366 °C to 375 °C). The SO$_2$ resistance of Ce/In-CHA-12 was also evaluated under the conditions with SO$_2$ feeding (Fig. S15B). In this case, the NOx conversion decreased slowly with time-on-stream, exhibiting a decreased value of 21.4% within 22 h for SO$_2$ feeding. The above results showed that the Ce/In-CHA-12 exhibited good water and sulfur resistances.

To further identify the roles of indium and cerium species on the catalytic performance of Ce/In-CHA catalysts in CH$_4$-SCR reaction, Arrhenius plots were drawn in Fig. 4A. Over In-CHA-12, the activation energy (Ea) for NOx reduction was 115.7 kJ/mol. The introduction of cerium species significantly reduced the Ea (74.3 kJ/mol) for NOx reduction on Ce/In-CHA-12, along with an increased reaction rate. Conversely, a low reaction rate was observed on Ce/CHA-12, accompanied by a low Ea (64.6 kJ/mol), possibly due to the promotional effect of Ce species in NOx activation. The above results suggested that the introduction of cerium species promoted the activation of NO and CH$_4$,

thus changing the pathway of NOx reduction, which was in good agreement with the results of the effect of NO$_2$ addition on the In-CHA-12 catalyst at low temperatures. As shown in Fig. 3A and Fig. S16A, the CH$_4$-SCR performance of the In-CHA-12 catalyst obviously decreased at 400 °C, separated by two activity temperature windows centering at 370 °C and 475 °C, respectively. As NO$_2$ plays a crucial role in the CH$_4$-SCR reaction [7,55], therefore, the effect of NO$_2$ addition on the In-CHA-12 catalyst performance was investigated at the temperatures of 370 °C and 475 °C, respectively (Fig. S17). At a low temperature of 370 °C, it was found that the addition of NO$_2$ enhanced the NOx conversion, while it had little effect on the CH$_4$-SCR performance at high temperature of 475 °C. At 370 °C, it should be noted that CH$_4$ conversion was hardly affected by NO$_2$ addition (Fig. S16B), while the fraction of CH$_4$ consumption assignable to SCR process (the selectivity index (α)) was significantly increased (Figs. S17A and B). These results suggested that NO$_2$ originated from NO oxidation help CH$_4$ activation via the breakage of the C-H bond, and thus enhanced the low-temperature CH$_4$-SCR activity [11,56]. At high temperatures, however, such enhancement on CH$_4$ activation induced by NO$_2$ addition was hardly observed (Figs. S17C and D), indicative of the occurrence of different CH$_4$-SCR pathway. The alternation of the reaction mechanism leads to a decrease in NOx conversion around 400 °C. Besides, an increase in the SiO$_2$/Al$_2$O$_3$ ratio significantly reduced the reaction rate for NOx reduction on Ce/In-CHA catalysts (Fig. 4B), accompanied by a decrease in the activation energy (Table S3). Such influence might be related to the change in indium species (InO$^+$ and In$_x$O$_y$ clusters), which would further affect the activation of CH$_4$.

To further confirm the role of NO$_2$ in the CH$_4$-SCR reaction, NO oxidation was evaluated on other OXZEO catalysts (Fig. 4C-D), the occurrence of which was enhanced by the modification with CeO$_2$ particularly at low temperatures. Therefore, it is reasonable that the Ce/In-CHA-12 catalyst exhibited higher activity and lower energy barrier for CH$_4$-SCR reaction than In-CHA-12. Furthermore, the SiO$_2$/Al$_2$O$_3$ ratio of the supports had minor effect on NO oxidation, with the order being Ce/In-CHA-12 ≈ Ce/In-CHA-20 > Ce/In-CHA-50 (Fig. 4E). Additionally, CH$_4$ activation is a crucial for the CH$_4$-SCR reaction, and
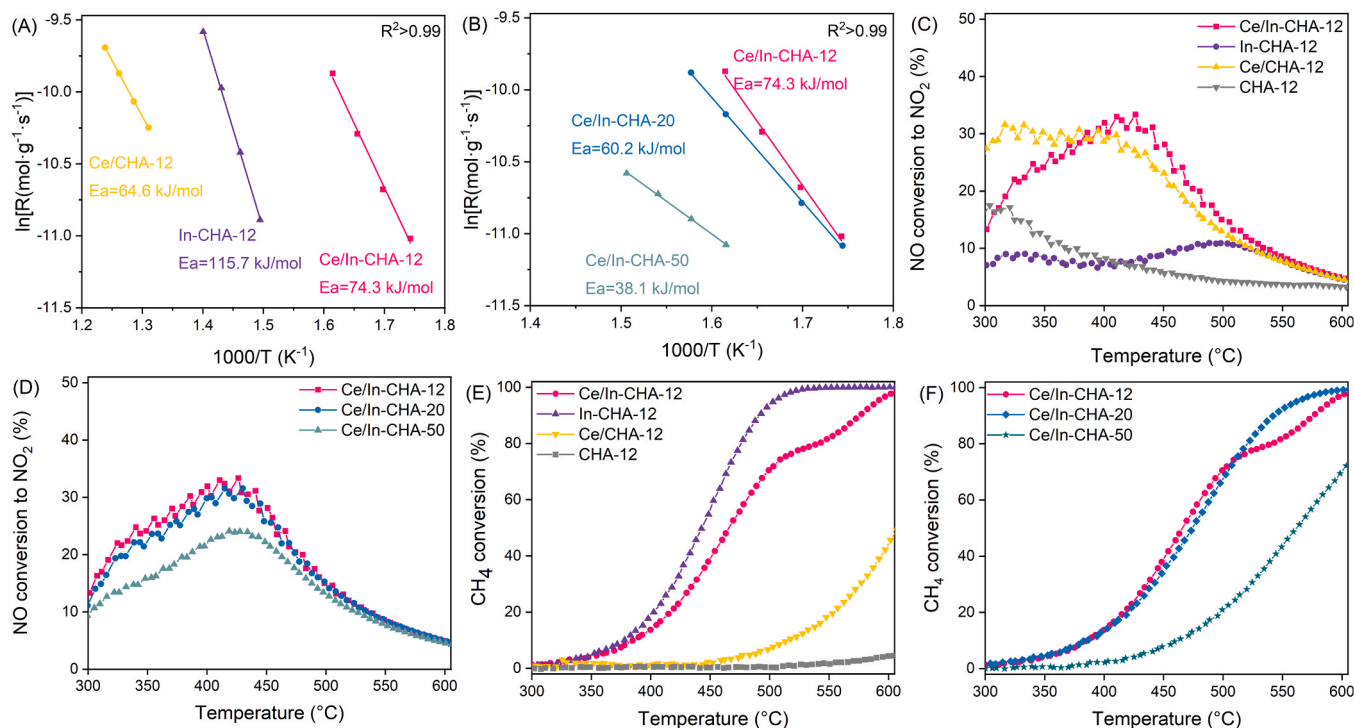

Fig. 4. Arrhenius plots for apparent activation energy over different catalysts in CH$_4$-SCR (A, B); Catalytic oxidation of NO to NO$_2$ (C, D) and catalytic oxidation of CH$_4$ to CO$_2$ (E, F) over the above samples.

therefore, the CH_4 oxidation performance of different catalysts was evaluated (Fig. 4E-F). The CHA-12 exhibited minimal CH_4 oxidation, and the Ce/CHA-12 catalyst achieved CH_4 conversion of less than ~40% at 600 °C. In contrast, In-CHA-12 catalyst exhibited the best CH_4 oxidation performance, achieving complete CH_4 oxidation at 500 °C, demonstrating the critical role of indium species in activating CH_4. Besides, the presence of CeO_2 on the surface of Ce/In-CHA-12 would hinder the direct oxidation of CH_4 at high temperatures to some extent. Additionally, the Ce/In-CHA-20 exhibited similar catalytic performance with Ce/In-CHA-12, while Ce/In-CHA-50 was the poorest.

Additionally, the role of different active sites in the reaction was further elucidated by investigating the reaction orders for NO and CH_4 (Fig. S19). The results indicated that the NO reaction order for In-CHA-12 was 0.83, whereas the NO reaction order for the Ce/In-CHA-12 catalyst was reduced to 0.21. Conversely, the reaction orders for CH_4 increased from -0.18 (In-CHA-12) to 0.41 (Ce/In-CHA-12). It suggested that CeO_2 could enhance the adsorption of NO on the catalyst but suppress the CH_4 adsorption. Comparing the reaction orders of NO and CH_4 on these catalysts, it was proposed that the adsorption of CH_4 on the surface of In-CHA-12 was stronger than that of NO, while the adsorption of NO on the surface of Ce/In-CHA-12 was stronger than that of CH_4. In summary, these results indicated that the role of CeO_2 was to activate NO, whereas the role of indium species was to activate CH_4 in the CH_4-SCR reaction.
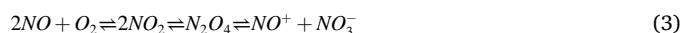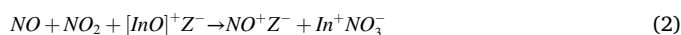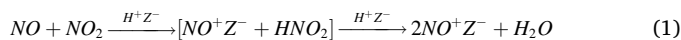
3.3. Reaction mechanism

The reaction mechanism of CH_4-SCR on these OXZEO catalysts was further investigated by in-situ DRIFTS. The roles of indium species and CeO_2 in activating CH_4 and NO were investigated firstly. Upon exposure to $CH_4 + O_2$, distinct peaks corresponding to methane (ν(C-H), 3015 cm^{-1}) and methoxy (νs(CH_3), 2933 cm^{-1}) were observed on the In-CHA-12 catalyst (Fig. 5A) [57,58]. This phenomenon underscored the remarkable ability of indium species to activate CH_4 and facilitate the cleavage of C-H bonds [59]. Besides, the exposure of NO + O_2 on the Ce/In-CHA-12 catalyst induced the formation of various intermediates, including nitrosonium ions (NO^+, 2198 cm^{-1}), monodentate nitrates (1536 cm^{-1}), and ionic nitrates (1368 cm^{-1}) [20,55,60,61]. This result confirmed the role of CeO_2 in promoting the oxidation of NO to form nitrate species and NO_2, which was recognized as pivotal steps in the CH_4-SCR reaction. Hence, these spectroscopic insights shed light on the distinctive roles played by indium species and CeO_2 in facilitating the activation and transformation of CH_4 and NO, respectively, further demonstrating their synergistic contributions to the CH_4-SCR reaction.

Fig. 6 and S20 showed the in-situ DRIFTS spectra obtained during the CH_4-SCR reaction on the OXZEO catalysts. In all these spectra, two bands were observed at 3595 and 3556 cm^{-1}, which were associated with OH groups associated with the 8-member and 6-member rings of the CHA structure, respectively (Fig. 6A) [7,23]. Besides, an additional band at 3652 cm^{-1} was observed on In/CHA-12 and Ce/In-CHA-12. This band likely arose from -OH groups bonded to In^{3+} cations and could be attributed to the equilibrium reaction involving neighboring InO^+ and H^+ cations [$InO^+ + H^+ \rightleftharpoons (InOH)^{2+}$]. This finding provided insight into the surface chemistry of the catalysts, particularly highlighting the interaction between In^{3+} cations and OH groups in In-CHA-12 [23].

The DRIFTS spectra also revealed the presence of several species, including CH_4, NO^+ ions, and adsorbed bridged nitrates. Besides, significant variations in the intensity of monodentate nitrates and ionic nitrates were observed on the In-CHA-12 and Ce/In-CHA-12. On the surface of Ce/In-CHA-12, the peaks due to nitrate species exhibited stronger intensity compared with that on In-CHA-12, which was mainly related to its higher ability for NO oxidation (Fig. 3C and D). Previous studies have shown that NO^+ and H_2O are generated at the Brønsted acid sites (Eq. 1), while NO^+ and NO_3^- are formed on $[InO]^+Z^-$ species within the zeolite (Eq. 2) and on CeO_2 species (Eq. 3), respectively [20,23]. The results indicated that both CeO_2 and InO^+ species play roles in promoting the production of NO^+ and nitrate species during the CH_4-SCR reaction. Furthermore, a band at 1560 cm^{-1} attributed to CH_3NO_2 was also observed on these catalysts [30,62], which was due to the activation of CH_4 at the InO^+ site (Fig. 5A). As a result, the Ce/In-CHA-12 catalyst, which contains both CeO_2 and InO^+ species, exhibits the best CH_4-SCR performance among the OXZEO catalysts.

$$NO + NO_2 \xrightarrow{H^+Z^-} [NO^+Z^- + HNO_2] \xrightarrow{H^+Z^-} 2NO^+Z^- + H_2O \quad (1)$$

$$NO + NO_2 + [InO]^+Z^- \rightarrow NO^+Z^- + In^+NO_3^- \quad (2)$$

$$2NO + O_2 \rightleftharpoons 2NO_2 \rightleftharpoons N_2O_4 \rightleftharpoons NO^+ + NO_3^- \quad (3)$$

After preabsorbing the catalysts with NO + O_2 for 30 min at 400 °C, the adsorbed NOx species, including NO^+ (2198 cm^{-1}), monodentate nitrates (1536 cm^{-1}), and ionic nitrates (1368 cm^{-1}), were observed on Ce/In-CHA-12 and Ce/CHA-12 catalysts. On the other hand, the In-CHA-12 catalyst exhibited new adsorbed NOx species, including bridged nitrates (1608 cm^{-1}) and bidentate nitrate species (1571 cm^{-1}) [20,23]. After N_2 purge for 15 min, the NO^+ (2198 cm^{-1}) completely disappeared on the Ce/In-CHA-12 catalyst, while the monodentate nitrate (1536 cm^{-1}) decreased significantly. However, the intensity of the peak at 1368 cm^{-1} remained essentially unchanged, indicating differences in the stability of various nitrate species. In contrast, the intensity of the nitrate (1608 and 1571 cm^{-1}) on the In-CHA-12 catalyst remained
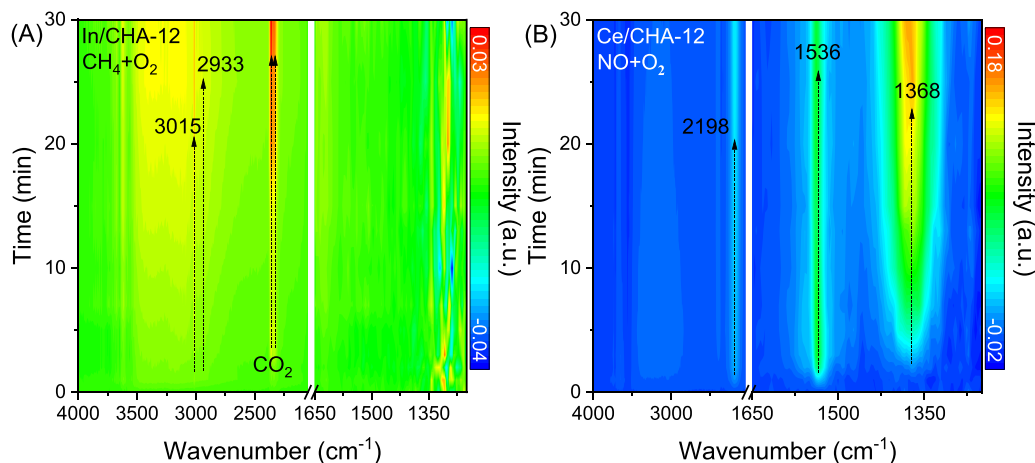

Fig. 5. In-situ DRIFTS spectra of CH_4 oxidation on In-CHA-12 at 400 °C for 30 min (A) and NO oxidation on Ce/CHA-12 at 400 °C for 30 min (B). Feed composition: 2000 ppm CH_4, 1200 ppm NO, and 4% O_2 in Ar balance.
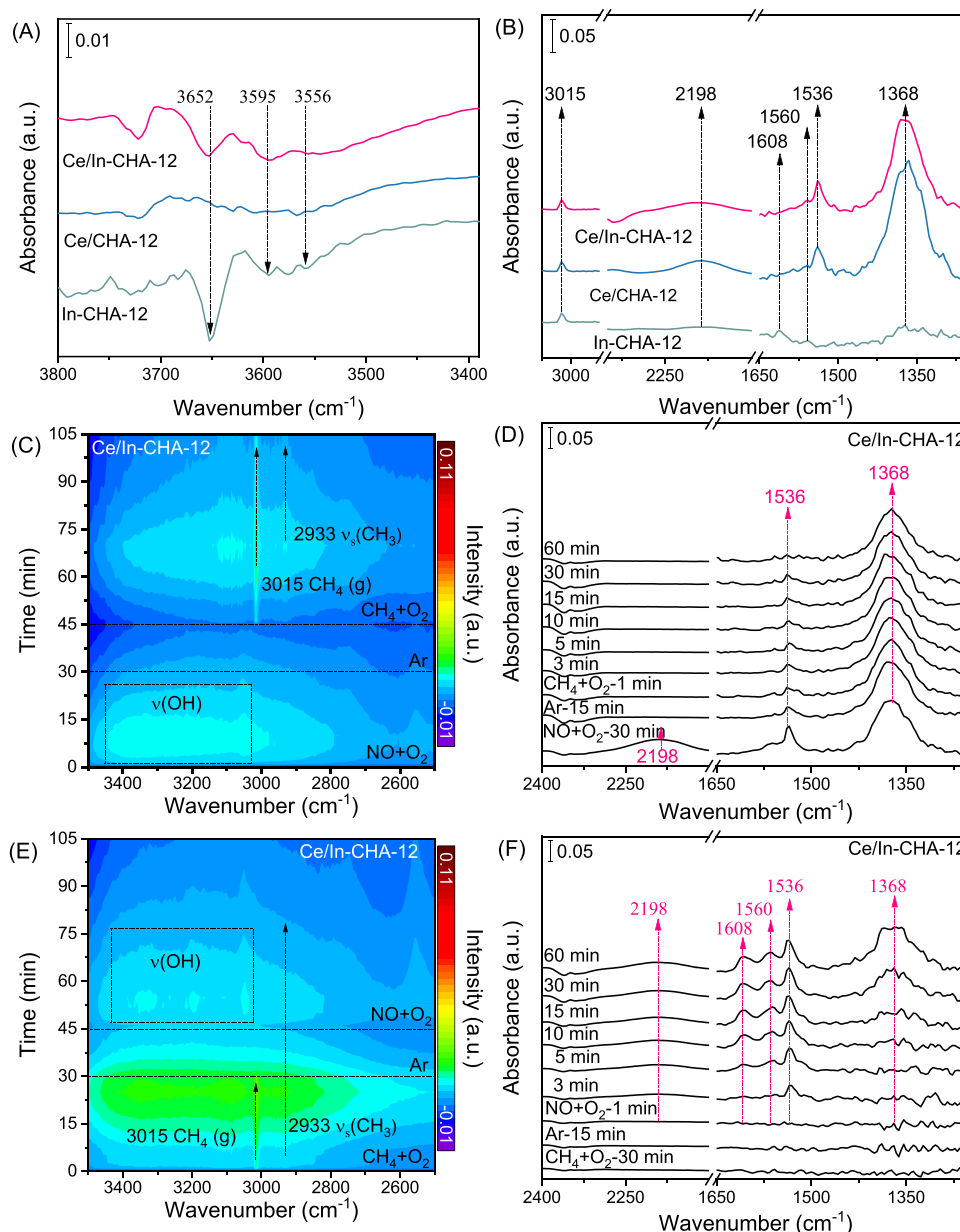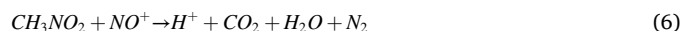
Fig. 6. In-situ DRIFTS spectra of CH$_4$-SCR on zeolite catalysts at 400 °C for 60 min (A, B). In situ DRIFTs for transient reaction of absorbed NO + O$_2$ with CH$_4$ + O$_2$ over Ce/In-CHA-12 catalyst at 400 °C. Spectra among (C) 3500–2500 cm^{-1} and (D) 2400–1250 cm^{-1}; In situ DRIFTs for transient reaction of preabsorbed CH$_4$ + O$_2$ with NO + O$_2$ over Ce/In-CHA-12 catalyst at 400 °C. Spectra among (E) 3500–2500 cm^{-1} and (F) 2400–1250 cm^{-1}; Reaction conditions: 10 mg catalysts, 2000 ppm CH$_4$, 1200 ppm NO, 4% O$_2$, Ar balance; Total flow rate = 40 mL/min.

relatively stable, which could be attributed to the complexation of NO$_3$ by InO$^+$ ions. When CH$_4$ + O$_2$ was introduced to the Ce/In-CHA-12 and Ce/CHA-12 catalysts, the peak at 1536 cm^{-1} further decreased. Weak adsorption peaks for CH$_4$ (3015 cm^{-1}) and CH$_3$O· (2933 cm^{-1}) appeared, while CH$_3$NO$_2$ was absent. In contrast, a peak corresponding to intermediate CH$_3$NO$_2$ (1560 cm^{-1}) was observed on the In-CHA-12 catalyst (Fig. S21B).

The reactivity of pre-adsorbed CH$_4$ toward NO + O$_2$ on these OXZEO catalysts was further investigated (Fig. 6E-F and S21E-H). After exposure to CH$_4$ + O$_2$, adsorbed CH$_4$ (3015 cm^{-1}) and CH$_3$O (2933 cm^{-1}) were observed on these catalysts. After purging with N$_2$ for 15 min, the peak at 3015 cm^{-1} disappeared, but the faint peak of CH$_3$O·remained stable. After exposure to NO + O$_2$, various nitrate species (2198, 1608, 1536, and 1368 cm^{-1}) emerged on these catalysts. Simultaneously, CH$_3$NO$_2$ (1560 cm^{-1}) was observed on the Ce/In-CHA-12 and In-CHA-12 catalysts. It indicated that the involvement of InO$^+$ species in activating

CH$_4$ (Eq. 4), followed by a reaction with nitrate species to form CH$_3$NO$_2$ (Eq. 5). Importantly, no cyanide (CN) or isocyanate (NCO) species were observed, suggesting that N$_2$ was produced by the further reaction of CH$_3$NO$_2$ with NO$^+$ (Eq. 6).

$$CH_4 + InO^+ \rightarrow CH_3InO + H^+ \tag{4}$$

$$CH_3InO + NO_3^- + 2H^+ \rightarrow CH_3NO_2 + InO^+ + H_2O \tag{5}$$

$$CH_3NO_2 + NO^+ \rightarrow H^+ + CO_2 + H_2O + N_2 \tag{6}$$

3.4. Discussion

In general, the CH$_4$-SCR reaction involves the activation of methane to reactive oxygenated hydrocarbons, which further react with NOx and/or nitrates to yield organo−NOx compounds, and subsequently
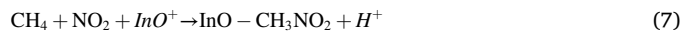
reduce to generate N_2, CO_2, and H_2O. Notably, the oxidation of NOx further enhances the activation of methane, leading to the formation of reactive oxygenated hydrocarbons, thus contributing to improved NOx reduction. In this work, a bifunctional Ce/In-CHA OXZEO catalyst was synthesized, with indium species confined within the CHA zeolite and CeO_2 assembled onto the surface of CHA zeolite, achieving nanoscale-separation of active sites (Fig. 1). XPS, H_2-TPR, and UV–vis results revealed that the indium species existed in the form of InO^+ and In_xO_y, while the cerium species were mainly present as CeO_2 on the outer surface of the zeolite. The indium species on the outer surface of CHA were slightly affected by CeO_2, resulting in the appearance of In_xO_y species (Fig. 2B). Notably, the Brønsted acid sites in CHA served as anchoring sites for InO^+ species, and CHA zeolite with lower SiO_2/Al_2O_3 ratio contained a higher concentration of Brønsted acid sites, thereby accommodating more InO^+ species.

During the CH_4-SCR reaction on the In-CHA-12 catalyst (Fig. 3A and S16), notably, the NOx conversion curve exhibited two distinctive peaks resembling a double volcano, indicating the existence of two separate reaction pathways at low and high temperatures, respectively. At low temperatures (below 400 °C), the NOx conversion of In-CHA-12 improved significantly in the presence of NO_2, while the high-temperature performance remained essentially unchanged, suggesting that the promotion effect of NO_2 on CH_4 activation mainly occurred at lower temperatures (Fig. S16 and S17). In other words, the reaction pathway of NO_2 assisted CH_4-SCR occurred at low temperatures, as had been expected. The Ce/CHA-12 catalyst demonstrated high efficiency for NO oxidation, mainly due to the superior redox activity of cerium species. Consequently, the core-shell Ce/In-CHA OXZEO catalyst demonstrated excellent catalytic performance in the CH_4-SCR reaction, achieving 100% NOx conversion at 395 °C, which could be attributed to the synergistic effect of different functional sites. Furthermore, this catalyst exhibited remarkable stability and maintained significant catalytic activity even in the presence of water vapor at high GHSV.

Over the Ce/In-CHA-12, the NO_2 assisted CH_4-SCR at a temperature below 400 °C was further confirmed by kinetic studies (Fig. 4A). Over this catalyst, it should be noted that the Ea value for CH_4-SCR was much lower than that of In-CHA-12, and being similar to that of Ce/CHA-12. This result clearly indicates that the CH_4-SCR performance is closely related to the oxidizing of NO to form NO_2 (Fig. 4C). Among the Ce/In-CHA samples with different SiO_2/Al_2O_3 ratio, a decreased value of Ea is related to the increase in oxidation properties due to the increase in the content of bulk In_2O_3 which correspondingly leads to a decrease in the reaction rate.

According to DRIFTs experiments, the CH_3NO_2 intermediates can be found on the surface of both In-CHA-12 and Ce/In-CHA-12 catalysts in the reactivity of the adsorbed $CH_4 + O_2$ species towards $NO + O_2$ (Fig. 6F and S21F), which can indicate that methane needs to be preferentially activated in the CH_4-SCR process. In addition, the pattern of CH_4 activation changed with increasing temperature due to kinetic and thermodynamic effects, indicating that the CH_4-SCR pathways of Ce/In-CHA OXZEO are divided into two types (Scheme 1). At low temperatures (below 400 °C), NO was oxidized at the CeO_2 site to form NO_2, and then

CH_4 was directly activated by NO_2 with strong oxidizing properties to form the CH_3NO_2 species (Eq. 7) at InO^+ sites, following the NO_2 assisted CH_4-SCR pathway. At temperatures above 400 °C, such NO_2 assisted CH_4-SCR pathway was suppressed which was due to the kinetic limitation of NO oxidation (Fig. 4C). In this case, methane needs to be activated by O_2 to form CH_3·in the InO^+ site before it reacts with the nitrate species to form CH_3NO_2 intermediates (Eqs. 4–6). Furthermore, the high-temperature performance of In-CHA-12 was severely suppressed in the presence of water, which was possibly due to the inability of the generated $In(OH)_2^+$ $[InO^+ + H_2O \rightleftharpoons In(OH)_2^+]$ to activate CH_4.

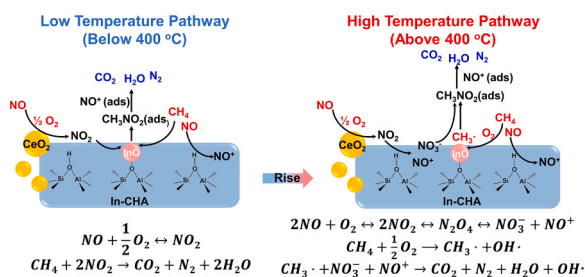$$CH_4 + NO_2 + InO^+ \rightarrow InO - CH_3NO_2 + H^+ \qquad (7)$$

The coupling of oxidation and reduction sites by separating active sites is a crucial strategy for enhancing the efficiency of the CH_4-SCR catalyst. Tandem catalysis is achieved in this approach, the CeO_2 site plays a pivotal role in oxidizing NO to NO_2 and generating nitrate species, which can react with activated methane at InO^+ to produce the key intermediate CH_3NO_2, and ultimately reducing NOx to N_2 and H_2O. Designing efficient CH_4-SCR catalysts hinges on two critical factors: firstly, the oxidation site must exhibit excellent NO oxidation activity, and secondly, the reduction site should be designed to minimize over-oxidation of CH_4, which can lead to lower reductant levels. Besides, the catalysts should be designed to minimize the effect of water, which can lead to the reduction site deactivation. The CHA zeolite served as an ideal support for the distribution of these different components. Specifically, the reduction component (indium species) is accommodated within the zeolite pores, while the oxidation component (CeO_2) is supported on the outer surface, essentially no interaction. Consequently, the tandem synergistic effect of these redox components significantly improved the performance of the Ce/In-CHA-12 catalyst in the CH_4-SCR reaction.

4. Conclusion

In summary, a Ce/In-CHA-12 OXZEO catalyst has been successfully developed, and it has demonstrated high performance in CH_4-SCR. Comprehensive characterizations revealed that on the Ce/In-CHA OXZEO catalysts, indium species predominantly existed in the form of InO^+ and In_xO_y within the CHA zeolite framework, while CeO_2 primarily resided as an external layer. During the CH_4-SCR reaction, CeO_2 promoted NO oxidation to form NO_2 and nitrate species, which further directly activated CH_4 or reacted with methyl at low and high temperatures, respectively, thus facilitating the formation of the key intermediate CH_3NO_2. Besides, the SiO_2/Al_2O_3 ratio of CHA zeolite has significant influence on the chemical properties of CHA zeolites, such as Brønsted acid sites, which remarkably affected the anchoring of InO^+ species. Specifically, the Ce/In-CHA-12 with a low SiO_2/Al_2O_3 ratio achieved 100% NOx conversion at 395 and 475 °C in the absence and presence of 10% H_2O, respectively, in the CH_4-SCR reaction, while having a lower activation energy (74.3 kJ/mol) and the highest reaction rate. This work provides a straightforward approach for designing efficient catalysts for simultaneously control NOx and CH_4 emissions.

CRediT authorship contribution statement

Chunlei Zhang: Data curation, Investigation, Formal analysis, Writing original draft, Writing - review & editing. **Guangyan Xu:** Conceptualization, Methodology, Validation, Writing - review & editing, Project administration. **Yanshuang Zhang:** Data curation, Investigation, Validation. **Chuang Chang:** Data curation, Investigation, Validation. **Miao Jiang:** Data curation, Investigation, Validation. **Luna Ruan:** Data curation, Investigation, Validation. **Min Xiao:** Data curation, Investigation, Validation. **Zidi Yan:** Conceptualization, Methodology, Validation. **Yunbo Yu:** Conceptualization, Methodology, Validation, Writing - review & editing, Project administration. **Hong He:**

Scheme 1. Proposed reaction pathway of CH_4-SCR on the Ce/In-CHA-12 OXZEO zeolite.

Conceptualization, Writing - review & editing, Project administration, Resources, Supervision.

Declaration of Competing Interest

The authors declare that they have no known competing financial interests or personal relationships that could have appeared to influence the work reported in this paper.

Data Availability

Data will be made available on request.

Appendix A. Supplementary material

Additional experimental procedures/data are provided in the Supplementary Information:

Detail information of TEM images, HAADF image and EDX elemental mapping, XRD results, N_2 adsorption-desorption isotherms, NH_3-TPD results, XPS spectra, H_2-TPR results, UV–vis absorption spectra, catalytic performance of different samples under different conditions, activation energy and reaction rate, in situ DRIFTS experiment.

Appendix A. Supporting information

Supplementary data associated with this article can be found in the online version at doi:10.1016/j.apcatb.2024.123820.

References

[1] J.B. Lim, J. Shin, N.H. Ahn, I. Heo, S.B. Hong, Selective catalytic reduction of NO with CH_4 over cobalt-exchanged cage-based, small-pore zeolites with different framework structures, Appl. Catal. B-Environ. 267 (2020) 118710.

[2] K. Li, H. Wang, L. Chen, J. Li, F. Dong, Synergistic degradation of NO and C_7H_8 for inhibition of O_3 generation, Appl. Catal. B-Environ. 312 (2022) 121423.

[3] G. Xu, J. Ma, G. He, Y. Yu, H. He, An alumina-supported silver catalyst with high water tolerance for H_2 assisted C_3H_6-SCR of NOx, Appl. Catal. B-Environ. 207 (2017) 60–71.

[4] Y. Yu, J. Zhao, Y. Yan, X. Han, H. He, A cyclic reaction pathway triggered by ammonia for the selective catalytic reduction of NOx by ethanol over Ag/Al_2O_3, Appl. Catal. B-Environ., 136- 137 (2013) 103–111.

[5] G. Xu, J. Ma, L. Wang, W. Xie, J. Liu, Y. Yu, H. He, Insight into the origin of sulfur tolerance of Ag/Al_2O_3 in the H_2-C_3H_6-SCR of NOx, Appl. Catal. B-Environ. 244 (2019) 909–918.

[6] V.I. Pârvulescu, P. Grange, B. Delmon, Catalytic removal of NO, Catal. Today 46 (1998) 233–316.

[7] R. Charrad, H.E. Solt, A. Domjan, F. Ayari, M. Mhamdi, J. Valyon, F. Lonyi, Selective catalytic reduction of NO by methane over Co,H-SSZ-13 catalysts: Types and catalytic functions of active Co sites, J. Catal. 385 (2020) 87–102.

[8] S. Han, X. Tang, Y. Ma, Q. Wu, J. Shi, J. Li, X. Meng, A. Zheng, F.-S. Xiao, Design of cobalt–amine complex as an efficient structure-directing agent for one-pot synthesis of Co-SSZ-13 zeolite, J. Phys. Chem. C 125 (2021) 16343–16349.

[9] E.M. Sadovskaya, A.P. Suknev, L.G. Pinaeva, V.B. Goncharov, B.S. Bal'zhinimaev, C. Chupin, J. Pérez-Ramírez, C. Mirodatos, Mechanism and kinetics of the selective NO reduction over Co-ZSM-5 studied by the SSITKA technique: 2. Reactivity of NOx-adsorbed species with methane, J. Catal. 225 (2004) 179–189.

[10] E.A. Lombardo, G.A. Sill, J.L. d'Itri, W.K. Hall, The possible role of nitromethane in the SCR of NOx with CH_4 over M-ZSM5 (M = Co, H, Fe, Cu), J. Catal. 173 (1998) 440–449.

[11] T. Sowade, F.-W. Schütze, H. Berndt, W. Grünert, Kinetic reaction models for the selective reduction of NO by methane over multifunctional zeolite-based redox catalysts, Chem. Eng. Technol. 27 (2004) 1277–1289.

[12] D. Jiang, K. Khivantsev, Y. Wang, Low-temperature methane oxidation for efficient emission control in natural gas vehicles: Pd and beyond, ACS Catal. 10 (2020) 14304–14314.

[13] E. Kikuchi, M. Ogura, I. Terasaki, Y. Goto, Selective reduction of nitric oxide with methane on gallium and indium containing H-ZSM-5 catalysts: formation of active sites by solid-state ion exchange, J. Catal. 161 (1996) 465–470.

[14] H.P. Decolatti, A. Martínez-Hernández, L.B. Gutiérrez, G.A. Fuentes, J.M. Zamaro, Characterization of dispersed indium species obtained by thermal treatment of In–NH_4-zeolites and their impact on the SCR of NOx, Microporous Mesoporous Mater. 145 (2011) 41–50.

[15] J. Zhao, G. Zhang, J. He, Z. Wen, Z. Li, T. Gu, R. Ding, Y. Zhu, R. Zhu, Effect of preparation and reaction conditions on the performance of In/H-Beta for selective catalytic reduction of NOx with CH_4, Chemosphere 252 (2020) 126458.

[16] J. Zhao, Z. Li, R. Zhu, J. Zhang, R. Ding, Z. Wen, Y. Zhu, G. Zhang, B. Chen, Mechanism of the selective catalytic reduction of NOx with CH_4 on In/H-beta, Catal. Sci. Technol. 11 (2021) 5050–5061.

[17] H. Berndt, F.W. Schütze, M. Richter, T. Sowade, W. Grünert, Selective catalytic reduction of NO under lean conditions by methane and propane over indium/cerium-promoted zeolites, Appl. Catal. B-Environ. 40 (2003) 51–67.

[18] J. Zhao, L. Dong, Y. Wang, J. Zhang, R. Zhu, C. Li, M. Hong, Amino-acid modulated hierarchical In/H-Beta zeolites for selective catalytic reduction of NO with CH_4 in the presence of H_2O and SO_2, Nanoscale 14 (2022) 5915–5928.

[19] T. Sowade, C. Schmidt, F.W. Schütze, H. Berndt, W. Grünert, Relations between structure and catalytic activity of Ce-In-ZSM-5 catalysts for the selective reduction of NO by methane: I. The In-ZSM-5 system, J. Catal. 214 (2003) 100–112.

[20] F. Lónyi, H.E. Solt, J. Valyon, H. Decolatti, L.B. Gutierrez, E. Miró, An operando DRIFTS study of the active sites and the active intermediates of the NO-SCR reaction by methane over In,H- and In,Pd,H-zeolite catalysts, Appl. Catal. B-Environ. 100 (2010) 133–142.

[21] T. Sowade, T. Liese, C. Schmidt, F.W. Schütze, X. Yu, H. Berndt, W. Grünert, Relations between structure and catalytic activity of Ce–In-ZSM-5 catalysts for the selective reduction of NO by methane: II. Interplay between the CeO_2 promoter and different indium sites, J. Catal. 225 (2004) 105–115.

[22] A. Kubacka, J. Janas, B. Sulikowski, In/Co-ferrierite: a highly active catalyst for the CH_4-SCR NO process under presence of steam, Appl. Catal. B-Environ. 69 (2006) 43–48.

[23] F. Lónyi, H.E. Solt, J. Valyon, A. Boix, L.B. Gutierrez, The activation of NO and CH_4 for NO-SCR reaction over In- and Co-containing H-ZSM-5 catalysts, J. Mol. Catal. A: Chem. 345 (2011) 75–80.

[24] B. Gil, J. Janas, E. Włoch, Z. Olejniczak, J. Datka, B. Sulikowski, The influence of the initial acidity of HFER on the status of Co species and catalytic performance of CoFER and InCoFER in CH_4-SCR-NO, Catal. Today 137 (2008) 174–178.

[25] J. Yang, Y.P. Chang, W.L. Dai, G.J. Wu, N.J. Guan, L.D. Li, Ru-In/H-SSZ-13 for the selective reduction of nitric oxide by methane: Insights from temperature-programmed desorption studies, Appl. Catal. B-Environ. 236 (2018) 404–412.

[26] N. Li, B. Huang, X. Dong, J. Luo, Y. Wang, H. Wang, D. Miao, Y. Pan, F. Jiao, J. Xiao, Z. Qu, Bifunctional zeolites-silver catalyst enabled tandem oxidation of formaldehyde at low temperatures, Nat. Commun. 13 (2022) 2209.

[27] J. Zecevic, G. Vanbutsele, K.P. de Jong, J.A. Martens, Nanoscale intimacy in bifunctional catalysts for selective conversion of hydrocarbons, Nature 528 (2015), 245-+.

[28] W. Zhou, J. Kang, K. Cheng, S. He, J. Shi, C. Zhou, Q. Zhang, J. Chen, L. Peng, M. Chen, Y. Wang, Direct conversion of syngas into methyl acetate, ethanol, and ethylene by relay catalysis via the intermediate dimethyl ether, Angew. Chem., Int. Ed. 57 (2018) 12012–12016.

[29] T. Maunula, J. Ahola, H. Hamada, Reaction mechanism and microkinetic model for the binary catalyst combination of In/ZSM-5 and Pt/Al_2O_3 for NOx reduction by methane under lean conditions, Ind. Eng. Chem. Res. 46 (2007) 2715–2725.

[30] F.J. Huang, W. Hu, J.J. Chen, Y. Wu, P.F. Qu, S.D. Yuan, L. Zhong, Y.Q. Chen, Insight into enhancement of NO reduction with methane by multifunctional catalysis over a mixture of Ce/HZSM-5 and CoOx in excess of oxygen, Ind. Eng. Chem. Res. 57 (2018) 13312–13317.

[31] M. Zhao, J. Zhao, R. Ding, R. Zhu, H. Li, Z. Li, J. Zhang, Y. Zhu, H. Li, Insights into the superior resistance of In-Co_3O_4-Ga_2O_3/H-Beta to SO_2 and H_2O in the selective catalytic reduction of NOx by CH_4, J. Colloid Interface Sci. 626 (2022) 89–100.

[32] Y. Zhang, Y. Yu, H. He, Oxygen vacancies on nanosized ceria govern the NOx storage capacity of NSR catalysts, Catal. Sci. Technol. 6 (2016) 3950–3962.

[33] C. Peng, R. Yan, Y. Mi, G. Li, Y. Zheng, Y. Luo, J. Liang, W. Liu, Z. Li, D. Wu, X. Wang, H. Peng, Toward rational design of a novel hierarchical porous Cu-SSZ-13 catalyst with boosted low-temperature NOx reduction performance, J. Catal. 401 (2021) 309–320.

[34] J. Zhang, Y. Shan, L. Zhang, J. Du, H. He, S. Han, C. Lei, S. Wang, W. Fan, Z. Feng, X. Liu, X. Meng, F.-S. Xiao, Importance of controllable Al sites in CHA framework by crystallization pathways for NH_3-SCR reaction, Appl. Catal. B-Environ. 277 (2020) 119193.

[35] G. Zhao, X. Pan, Z. Zhang, Y. Liu, Y. Lu, A thin-felt Pd–MgO–Al_2O_3/Al-fiber catalyst for catalytic combustion of methane with resistance to water-vapor poisoning, J. Catal. 384 (2020) 122–135.

[36] K. Zhang, Q. Meng, H. Wu, J. Yan, X. Mei, P. An, L. Zheng, J. Zhang, M. He, B. Han, Selective Hydrodeoxygenation of Aromatics to Cyclohexanols over Ru Single Atoms Supported on CeO_2, J. Am. Chem. Soc. 144 (2022) 20834–20846.

[37] P.A.S. Moura, E. Rodríguez-Aguado, D.A.S. Maia, D.C. Melo, R. Singh, S. Valencia, P.A. Webley, F. Rey, M. Bastos-Neto, E. Rodríguez-Castellón, D.C.S. Azevedo, Water adsorption and hydrothermal stability of CHA zeolites with different Si/Al ratios and compensating cations, Catal. Today 391 (2022) 99–108.

[38] C. Fan, Z. Chen, L. Pang, S. Ming, X. Zhang, K.B. Albert, P. Liu, H. Chen, T. Li, The influence of Si/Al ratio on the catalytic property and hydrothermal stability of Cu-SSZ-13 catalysts for NH_3-SCR, Appl. Catal., A 550 (2018) 256–265.

[39] L. Chai, X. Wang, Y. Hu, X. Li, S. Huang, J. Pan, J. Qian, X. Sun, In-MOF-derived hierarchically hollow carbon nanostraws for advanced zinc-iodine batteries, Adv. Sci. 9 (2022) 2105063.

[40] K. Shen, W. Qian, N. Wang, C. Su, F. Wei, Fabrication of c-Axis oriented ZSM-5 hollow fibers based on an in situ solid–solid transformation mechanism, J. Am. Chem. Soc. 135 (2013) 15322–15325.

[41] T. Wang, C. Yang, P. Gao, S. Zhou, S. Li, H. Wang, Y. Sun, ZnZrOx integrated with chain-like nanocrystal HZSM-5 as efficient catalysts for aromatics synthesis from CO2 hydrogenation, Appl. Catal. B-Environ. 286 (2021) 119929.

[42] J. Du, X. Shi, Y. Shan, W. Zhang, Y. Yu, W. Shan, H. He, Investigation of suitable templates for one-pot-synthesized Cu-SAPO-34 in NOx abatement from diesel vehicle exhaust, Environ. Sci. Technol. 54 (2020) 7870–7878.

[43] D. Wang, F. Gao, C.H.F. Peden, J. Li, K. Kamasamudram, W.S. Epling, Selective catalytic reduction of NOx with NH3 over a Cu-SSZ-13 catalyst prepared by a solid-state ion-exchange method, ChemCatChem 6 (2014) 1579–1583.

[44] F. Gao, Y. Wang, N.M. Washton, M. Kollár, J. Szanyi, C.H.F. Peden, Effects of alkali and alkaline earth cocations on the activity and hydrothermal stability of Cu/SSZ-13 NH3–SCR catalysts, ACS Catal. 5 (2015) 6780–6791.

[45] F. Lónyi, H.E. Solt, J. Valyon, A. Boix, L.B. Gutierrez, The SCR of NO with methane over In,H- and Co,In,H-ZSM-5 catalysts: The promotional effect of cobalt, Appl. Catal. B-Environ. 117-118 (2012) 212–223.

[46] Z. Maeno, S. Yasumura, C. Liu, T. Toyao, K. Kon, A. Nakayama, J.-y Hasegawa, K.-i Shimizu, Experimental and theoretical study of multinuclear indium–oxo clusters in CHA zeolite for CH4 activation at room temperature, Phys. Chem. Chem. Phys. 21 (2019) 13415–13427.

[47] C. Wang, Y. Han, M. Tian, L. Li, J. Lin, X. Wang, T. Zhang, Main-group catalysts with atomically dispersed in sites for highly efficient oxidative dehydrogenation, J. Am. Chem. Soc. 144 (2022) 16855–16865.

[48] A.A. Gabrienko, S.S. Arzumanov, I.B. Moroz, I.P. Prosvirin, A.V. Toktarev, W. Wang, A.G. Stepanov, Methane activation on in-modified ZSM-5: the state of indium in the zeolite and pathways of methane transformation to surface species, J. Phys. Chem. C 118 (2014) 8034–8043.

[49] Y. Shi, J. Pu, L. Gao, S. Shan, Selective catalytic reduction of NO with NH3 and CH4 over zeolite supported indium-cerium bimetallic catalysts for lean-burn natural gas engines, Chem. Eng. J. 403 (2021) 126394.

[50] C. Liu, L. Gui, J.-J. Zheng, Y.-Q. Xu, B. Song, L. Yi, Y. Jia, A. Taledaohan, Y. Wang, X. Gao, Z.-Y. Qiao, H. Wang, Z. Tang, Intrinsic Strain-Mediated Ultrathin Ceria Nanoantioxidant, J. Am. Chem. Soc. 145 (2023) 19086–19097.

[51] M. Fan, Q. Zou, J. Liu, Y. Chen, J. Zhu, S. Shen, Enhanced catalytic oxidation of dichloromethane by a surfactant-modified CeO2@TiO2 core–shell nanostructured catalyst, J. Rare Earths 41 (2023) 1031–1041.

[52] Z. Di, H. Wang, R. Zhang, H. Chen, Y. Wei, J. Jia, ZSM-5 core–shell structured catalyst for enhancing low-temperature NH3-SCR efficiency and poisoning resistance, Appl. Catal. A 630 (2022) 118438.

[53] H. Pan, Y.F. Jian, Y.K. Yu, N.N. Chen, C. He, C. He, Promotional mechanism of propane on selective catalytic reduction of NOx by methane over In/H-BEA at low temperature, Appl. Surf. Sci. 390 (2016) 608–616.

[54] J. Yang, Y.P. Chang, W.L. Dai, G.J. Wu, N.J. Guan, L.D. Li, Bimetallic Cr-In/H-SSZ-13 for selective catalytic reduction of nitric oxide by methane, Chin. J. Catal. 39 (2018) 1004–1011.

[55] F. Lónyi, H.E. Solt, Z. Pászti, J. Valyon, Mechanism of NO-SCR by methane over Co, H-ZSM-5 and Co,H-mordenite catalysts, Appl. Catal. B-Environ., 150- 151 (2014) 218–229.

[56] H. Kato, C. Yokoyama, M. Misono, Rate-determining step of NO-CH4-O2 reaction catalyzed by Pd/H-ZSM-5, Catal. Lett. 47 (1997) 189–191.

[57] S. Tamm, H.H. Ingelsten, M. Skoglundh, A.E.C. Palmqvist, Mechanistic aspects of the selective catalytic reduction of NOx by dimethyl ether and methanol over γ-Al2O3, J. Catal. 276 (2010) 402–411.

[58] Z. Li, J. Wang, Y. Qu, H. Liu, C. Tang, S. Miao, Z. Feng, H. An, C. Li, Highly selective conversion of carbon dioxide to lower olefins, ACS Catal. 7 (2017) 8544–8548.

[59] S.S. Arzumanov, I.B. Moroz, D. Freude, J. Haase, A.G. Stepanov, Methane activation on in-modified ZSM-5 zeolite. H/D hydrogen exchange of the alkane with brønsted acid sites, J. Phys. Chem. C 118 (2014) 14427–14432.

[60] L. Castoldi, L. Lietti, P. Forzatti, S. Morandi, G. Ghiotti, F. Vindigni, The NOx storage-reduction on PtK/Al2O3 Lean NOx Trap catalyst, J. Catal. 276 (2010) 335–350.

[61] M.Y. Mihaylov, V.R. Zdravkova, E.Z. Ivanova, H.A. Aleksandrov, P.S. Petkov, G. N. Vayssilov, K.I. Hadjiivanov, Infrared spectra of surface nitrates: Revision of the current opinions based on the case study of ceria, J. Catal. 394 (2021) 245–258.

[62] H. Yasuda, T. Miyamoto, M. Misono, IR Study of Catalytic Reduction of NOx by Propene in the Presence of O2 over CeZSM-5 Zeolite, 1995, pp. 110–122.